The Effect of Hornerin Knockdown on Tumor Vasculature in Melanoma

A Technical Report submitted to the Department of Biomedical Engineering

Presented to the Faculty of the School of Engineering and Applied Science
University of Virginia • Charlottesville, Virginia

In Partial Fulfillment of the Requirements for the Degree
Bachelor of Science, School of Engineering

Zainab Aziz
Spring, 2021

Technical Project Team Members
Aishu Hombal
Saqib Rizvi

On my honor as a University Student, I have neither given nor received unauthorized aid on this assignment as defined by the Honor Guidelines for Thesis-Related Assignments.

Signature _____ Date _____
Zainab Aziz

Approved _____ Date _____
Dr. Kimberly Kelly, Department of Biomedical Engineering

The Effect of Hornerin Knockdown on Tumor Vasculature in Melanoma

Authors:
Aishu Hombal
Zainab Aziz
Saqib Rizvi
(Group 8D)
Jessica Hung
Dr. Kimberly Kelly

Words: 3555
Number of Figures: 7
Number of Tables: 0
Number of Equations: 0
Number of Supplements: 1
Number of References: 14

Email Signature Screenshot in Supplements

The Effect of Hornerin Knockdown on Tumor Vasculature in Melanoma

Aishu Hombal[a]. Zainab Aziz[a]. Saqib Rizvi[a]. Jessica Hung[a,b]. Kimberly Kelly[a,b,1].

[a] Department of Biomedical Engineering at the University of Virginia
[b] Kelly Lab, University of Virginia
[1] kkelly@virginia.edu

Abstract

Sustained angiogenesis, or blood vessel growth, is a characteristic of tumor cell metastasis.[1] The disordered tumor vasculature restricts the immune response into the tumor region.[2] One common angiogenic pathway is regulated by the vascular endothelial growth factor (VEGF). However, current anti-angiogenic therapies targeting VEGF often result in therapeutic resistance and tumor recurrence. Therefore, our lab previously identified a novel target, hornerin, as part of a compensatory angiogenic pathway. Hornerin is a VEGF independent protein, located on endothelial cells. Our lab's previous study, focused on pancreatic ductal adenocarcinoma (PDAC), showed that hornerin knockdown normalized vessel parameters, such as vessel volume fraction, vessel length density, fractal dimension, and radius distribution.[2] As such, one of the aims of our project was to replicate previous efforts and characterize the effect of hornerin knockdown on tumor vasculature in melanoma. As part of the characterization process, our first goal was to optimize an existing vessel analysis software called Rapid Analysis of Vessel Elements (RAVE). To address limitations of the software, we implemented batch-processing. Our optimization resulted in significantly quicker processing times compared to the original, manual processing. Afterwards, our second goal was to quantify the effects of hornerin knockdown on tumor vessel normalization in B16 melanoma. To this end, we confirmed the functionality of hornerin siRNA to decrease hornerin expression as well as characterized vessel parameters after hornerin knockdown. Our results indicated that there was a significant decrease in vessel parameters of vessel volume fraction, vessel length density, and fractal dimension between the hornerin siRNA and control group. Furthermore, hornerin knockdown reduced the vessel radius size compared to the control group. As such, we concluded that hornerin is an effect target for tumor vessel normalization through knockdown in regions where hornerin expression is significantly decreased. Future work includes characterization of the downstream immune response, as the tumor vasculature often restricts T-cell entry into the tumor region.

Keywords: Angiogenesis, VEGF, hornerin, melanoma, vessel parameters

Introduction

Cancer is one of the leading causes of death worldwide. In the United States alone, around two million cancer cases are diagnosed each year, resulting in approximately 600,000 deaths.[3] Melanoma is the most aggressive form of skin cancer and occurs due to genetic mutations in melanocytes, which are pigment producing cells.[4] Based on collected data, approximately 100,000 new melanoma cases are diagnosed each year in the United States, with around 7,000 expected deaths from the cancer. Moreover, the rates of melanoma occurence have been increasing over the last few decades across various age groups.[5] The high morbidity associated with cancers, particularly melanoma, conveys the need for novel treatments and innovative methods for deriving such treatments to ensure cancer patients receive the best possible care.

Cancer is characterized by rapid proliferation of cells, which can lead to the development of tumors, or masses of tissue. Cancerous tumors are malignant, which allows them to invade other tissues and spread cancer throughout the body. As such, cancer treatments strive to eliminate cancerous cells and the pathways that encourage the abnormal growth of cancer cells. One of these pathways involves the interaction between cancerous cells and the associated blood and lymphatic vessels. Angiogenesis is the development and maintenance of the vascular network that is necessary for tumor growth, and sustained angiogenesis permits tumor cell metastasis in cancer.[1] Blood vessels promote the growth of tumors by supporting the high oxygen and nutrient demands of the

tumors.[6] Additionally, cancer cells secrete elevated levels of pro-angiogenic factors, contributing to the development of a disordered vascular system containing immature and permeable blood vessels. The disordered tumor vasculature creates disrupted flow patterns and high interstitial fluid pressure that can impact the immune response, specifically by restricting T-cell entry into solid tumors.[6]

As such, cancer therapies often use an anti-angiogenic approach. Specifically, many therapies target the vascular endothelial growth factor (VEGF), which is a signaling protein that promotes the growth of blood vessels and is involved in restoring blood supply to oxygen-deprived cells and tissues.[7] In melanoma, anti-angiogenic therapies are mainly VEGF-targeted agents, including tyrosine kinase inhibitors and monoclonal antibodies.[8] While current monotherapies produce promising results, they often lead to only temporary remission due to the possibility of recurrence after completing treatment. The lack of long-term success can be attributed to the presence of compensatory pathways for angiogenesis.

A previous study used a phage display proteomics approach to identify hornerin, a VEGF independent protein located on endothelial cells, as part of a compensatory pathway for angiogenesis. siRNA, or small interfering RNA, is a form of noncoding RNA that operates within the RNA interference pathway to silence specific genes by inducing degradation of mRNA.[9] Hornerin siRNA is a form of siRNA that functions to downregulate, or knockdown, the expression of the hornerin protein. The study on pancreatic ductal carcinoma (PDAC) used hornerin knockdown to demonstrate the functional role of the protein in altering the following vessel parameters: vessel volume fraction, vessel length density, fractal dimension, which is a measure of tortuosity, and vessel radius distribution. Hornerin knockdown reduced leakiness in vessels, increased oxygenation, increased apoptosis of endothelial cells, and decreased the mentioned vessel parameters to normalize the tumor vasculature. Based on previous literature, hornerin was also found to be expressed in psoriatic and wounded skin, presenting it as a novel therapeutic target for vessel normalization in melanoma.[10]

Rapid Analysis of Vessel Elements (RAVE) is a software for image analysis of vessels that characterizes the aforementioned vessel parameters: vessel volume fraction (VVF), vessel length density (VLD), fractal dimension (FD), and radius distribution (RD).[11] The RAVE software aims to facilitate high-throughput image analysis of microvasculature environments with minimal introduction of analyst-specific variations. The software takes in an image, and performs multiple operations on it to collect and output the vessel parameters. To perform the analysis, the software binarizes the image based on a given threshold value. Post-processing, the number of white pixels helps calculate the vessel volume fraction. The image is subsequently skeletonized to create a one pixel wide outline of the vessel which is used for both the vessel radius and length density characterization.[11]

Prior to RAVE, vessel analysis softwares were commercially available as add-ons to microscope systems such Nikon's NIS-elements or Mauna Kei Technologies' Cellvizio, or manual analysis on tumor volume was conducted. However, many of the aforementioned options are costly and difficult to manipulate for distinct experimental analyses.[12] As such, a highly accessible and adaptable, open source analysis tool such as RAVE, is advantageous for vessel analysis.

Though RAVE presents many benefits, the software contains several limitations that decrease the sophistication and efficacy of the software. RAVE only allows for analysis of a single image at a time, which limits the potential for large scale analysis due to the time burden. Additionally, the software does not possess an output function or the ability to copy and paste, which, along with other minor bugs, decrease the functionality of the software. Therefore, the first aim of this research is to optimize the RAVE software by implementing batch processing, which allows for the selection of multiple images for analysis at once, and adding a function to create a single exportable .csv file to create a more user-friendly and efficient interface.

The second aim of this research is evaluating the effects of hornerin knockdown on tumor vasculature in melanoma to corroborate the findings of the PDAC study. The first sub-aim is to quantify hornerin expression to confirm that hornerin siRNA, which was used in the aforementioned PDAC study, is indeed a viable mechanism for hornerin knockdown. The second sub-aim is to characterize the vessel parameters using the optimized RAVE software in order to assess the efficacy of hornerin knockdown on normalization of tumor vasculature in melanoma.

Results

Optimization of Rapid Analysis of Vessel Elements Software

As discussed in the introduction, the existing RAVE software presented certain limitations, as it contained a loading bug, lacked the ability to output parameter data and required users to individually analyze each image. The optimization of RAVE, therefore, fixed

the initial loading error, implemented the ability for users to output vessel parameters in a .csv file, and allowed users to process multiple images using batch-processing. An example .csv output file is shown in Supplementary Figure 1. In order to compare the processing times between the manual and optimized RAVE, we analyzed three groups of five, ten, and twenty representative images using both versions. We then conducted unpaired, two-tailed t-tests between the processing times to show a statistically significant difference. As seen in Figure 1, the optimized RAVE resulted in significantly faster processing times for the groups of five, ten, and twenty images by 5, 6, and 8-fold, respectively, at a significance level of 0.005.

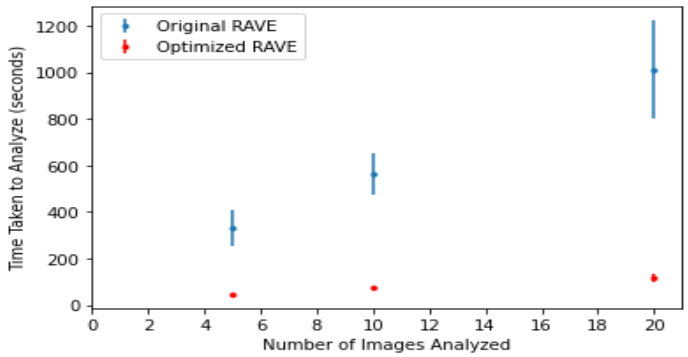

Figure 1: Processing Times in Manual and Optimized RAVE: Groups of 5, 10, and 20 images were analyzed to obtain the processing times for both the manual and optimized versions of RAVE. Unpaired, two-tailed t-tests were performed to show a statistically significant difference between the times. $p<0.005$.

Characterization of Hornerin Knockdown in B16 Melanoma

After completing optimization of the RAVE software, we moved forward with our second aim regarding the effect of hornerin knockdown on the tumor vasculature in B16 melanoma. The first sub-aim was to validate the efficacy of hornerin siRNA as a mechanism to knockdown hornerin and decrease hornerin expression. Our lab conducted tumor studies in which mice were injected with B16-OVA melanoma cells on Day 0. After the tumor size reached 110 mm^3, the mice were split into four experimental treatment groups: vehicle (no treatment), AV951 (a VEGF-inhibitor), hornerin siRNA, and scramble siRNA (which served as a negative control). The vehicle and AV951 treatments were administered using a daily gavage while the hornerin siRNA and scramble siRNA treatments were administered using intratumoral injections on alternating days. Treatments continued until Day 7, when tumors were extracted, sectioned, and stained. The tumor cross-sections were stained for hornerin, DAPI and CD31, a protein present in the endothelial linings.[13] Images of the sectioned and stained tumors were taken using confocal microscopy and representative images are shown in Figure 2. In particular, Figure 2 presents a qualitative view of the effect of hornerin knockdown on the tumor vasculature, namely normalization of the vessels, which will be further quantified in the next sub-aim with four vessel parameters.

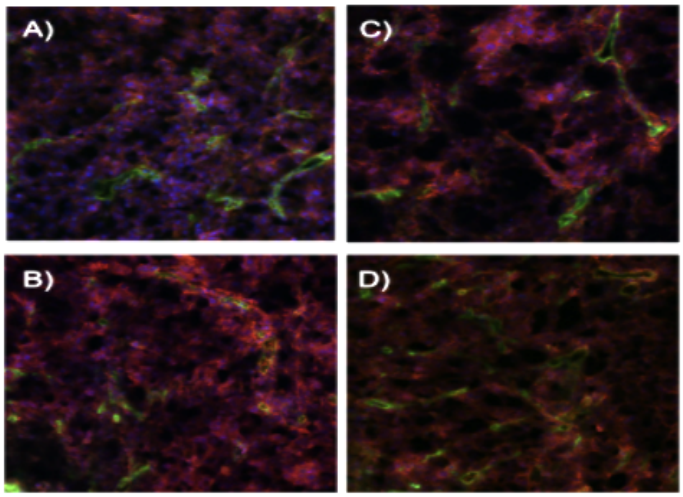

Figure 2: Representative Images from Confocal Imaging: Cross-sections were stained for hornerin, CD31, and DAPI across four experimental groups. Images taken at 20X. A) Vehicle, B) AV951, C) Hornerin siRNA, D) Scramble siRNA.

To assess the efficacy of hornerin siRNA in decreasing hornerin expression, we quantified the amount of hornerin using ImageJ. The hornerin stained channel was isolated on ImageJ and the mean grey intensity and integrated density were measured. Values for mean grey intensity and integrated density correlated with levels of hornerin expression. For example, lower values for mean gray intensity and integrated density would indicate lower levels of hornerin expression. These measurements were taken in the hornerin siRNA and scramble siRNA experimental groups and representative images of the hornerin stained vessels from these two groups are shown in Figure 3. In particular, Figure 3 qualitatively shows the difference in hornerin expression between the hornerin siRNA and scramble siRNA groups. Additionally, the hornerin siRNA groups were further separated based on the mouse and cage in which the mouse was treated. For example, siHrnr M1-1 indicated hornerin siRNA treatment in mouse 1 in cage 1 whereas siHrnr M3-2 represented hornerin siRNA treatment in mouse 3 in cage 2. The treatment locations were arbitrary but labeled and noted for our reference in analysis.

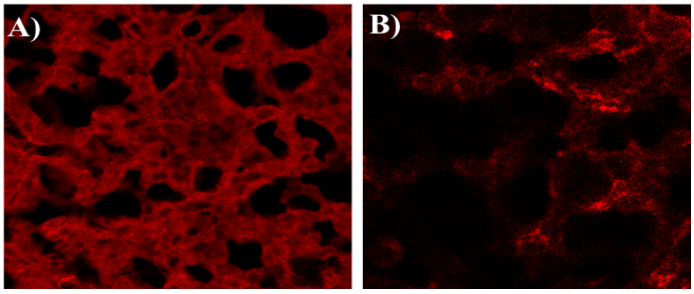

Figure 3: Representative Images from Confocal Imaging: Cross-sections were stained for hornerin and imaged at 20X. A) Hornerin siRNA, B) Scramble siRNA.

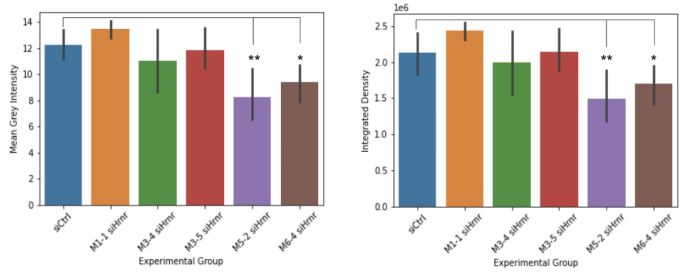

Figure 4: Hornerin Quantification: The left-most graph presents the mean grey intensity for various cross-sections while the right-most graph presents the integrated density for various cross-sections. Unpaired, two-tailed t-tests were conducted between the scramble and each of the hornerin knockdown groups. * $p<0.05$, ** $p<0.005$.

In Figure 4, the x-axis represents the experimental groups of scramble siRNA and the five hornerin siRNA groups. The y-axes represent the average mean gray intensity and average integrated density. Error bars were derived from standard deviations and the statistical significance was based on unpaired, two-tailed T-tests, conducted between the scramble siRNA and each of the hornerin siRNA groups. As seen in Figure 4, hornerin expression was reduced in endothelial cells in four of the five hornerin siRNA groups, namely M3-4, M3-5, M5-2, and M6-4, compared to the scramble siRNA group. The reduction in hornerin expression was significant in the M5-2 and M6-4 hornerin siRNA groups at a significance level of 0.005 and 0.05, respectively.

Characterization of Vessel Normalization in B16 Melanoma

With the results obtained regarding hornerin expression, we continued with our second sub-aim to obtain vessel parameters across the experimental groups. In addition to the vehicle (no treatment), AV951 (a VEGF inhibitor), and scramble siRNA experimental groups, we conducted vessel parameter analysis on the hornerin siRNA M5-2 and hornerin siRNA M6-4 groups, as these two groups had the most significant reduction in hornerin expression. Using the stained images obtained from microscopy earlier and the optimized RAVE software, we conducted vessel characterization to obtain the following vessel parameters: VVF, VLD, FD and RD. The vessel parameter data across the five experimental groups are shown in Figures 5 and 6. The error bars on the data were derived from standard deviations. Further, due to the differences in administration routes, we completed unpaired, two-tailed t-tests between the vehicle and AV951 groups and between the scramble siRNA and the two hornerin siRNA groups. All t-tests were conducted at a significance level of 0.05. As mentioned earlier, both the vehicle and AV951 groups received treatment with a daily gavage while the scramble siRNA and hornerin siRNA groups received treatment with intratumoral injections.

As seen in Figure 5A, the vessel volume fraction decreased between the vehicle and AV951 groups, though it was not significant at the tested significance level. The VVF significantly decreased between the hornerin siRNA M5-2 and scramble siRNA groups and there was a decrease between the hornerin siRNA M6-4 and scramble siRNA groups, though not significant. We obtained similar results for the vessel length density. As seen in Figure 5B, the vessel volume density decreased between the vehicle

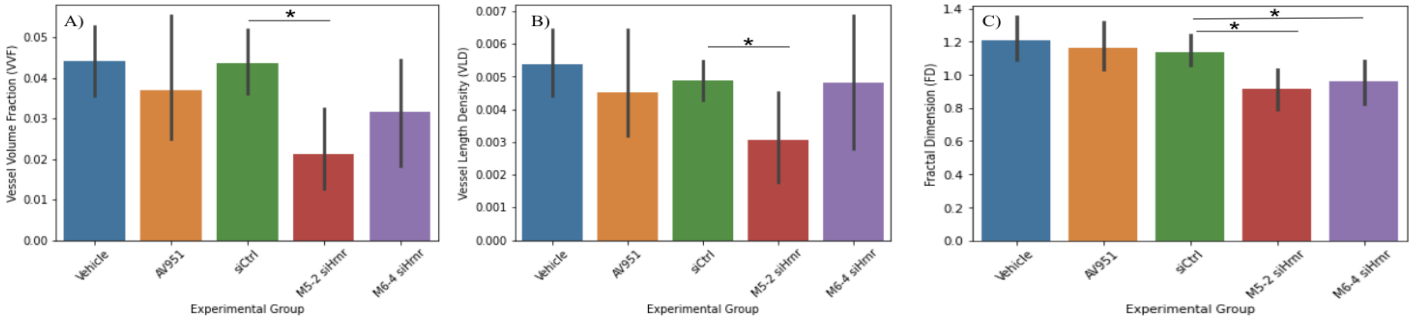

Figure 5: Melanoma Vessel Characterization: A) The graph presents the vessel volume fraction across all four experimental groups. B) The graph presents the vessel length density across all four experimental groups. C) The graph presents the fractal dimension across all four experimental groups. Unpaired, two-tailed T-tests were conducted between the vehicle and each of the remaining three experimental groups for each vessel parameter. * $p<0.05$

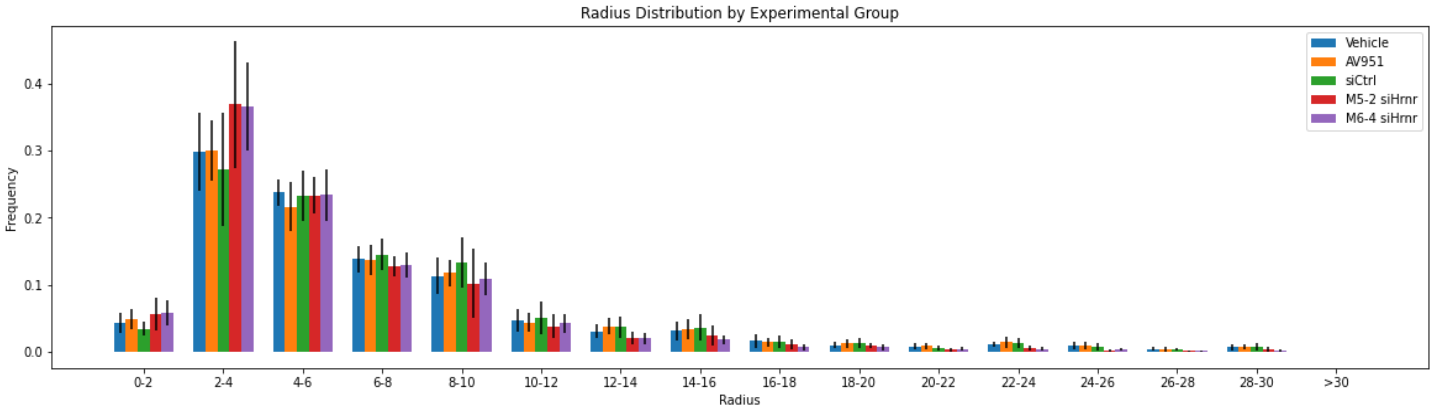

Figure 6: Melanoma Vessel Characterization Radius Distribution: The graph presents the radius distributions across all four experimental groups. Error bars were calculated with standard deviation. As seen in the Figure, there is a shift in radius frequency for the M5-2 siHrnr and M6-4 si-Hrnr groups towards smaller radii.

and AV951 groups, though it was not significant at the tested significance level. The VLD significantly decreased between the hornerin siRNA M5-2 and scramble siRNA groups and there was a decrease between the hornerin siRNA M6-4 and scramble siRNA groups, though not significant. As seen in Figure 5C, the fractal dimension decreased between the vehicle and AV951 groups, but it was not significant at the tested significance level. The FD significantly decreased between the hornerin siRNA M5-2 and scramble siRNA groups and between the hornerin siRNA M6-4 and scramble siRNA groups. The fourth vessel parameter of interest was the radius distribution. The RAVE analysis provided the frequencies of vessel parameters that fell between a range of radii. As seen in Figure 6, there was an overall reduction in vessel radius from larger to smaller vessels, specifically towards the 2-4 range, for both the hornerin siRNA M5-2 and hornerin siRNA M6-4 groups when compared to the scramble siRNA group.

Discussion

Though many common anti-angiogenic therapies target the VEGF pathway, these therapies often face resistance and result in tumor recurrence.[2] As such, other potential targets in the angiogenic pathway offer insight into novel therapeutic approaches. Our lab previously identified hornerin, a VEGF independent protein, as part of a compensatory angiogenic pathway. Previous studies in pancreatic ductal adenocarcinoma successfully demonstrated that hornerin knockdown resulted in tumor vasculature normalization.[2] As such, we replicated such efforts to demonstrate the effect of hornerin knockdown on the tumor vasculature in B16-OVA melanoma. Prior to characterization of the vasculature, we optimized an existing vessel analysis software, RAVE, to provide a more user-friendly and effective interface. In addition to correcting the initial loading error, we implemented an option that now allows users to summarize the results and export all results via a .csv file. Furthermore, we implemented batch processing, allowing users to analyze multiple images at once, which significantly reduced the processing times for analysis. These improvements now offer users with a more user-friendly interface as well as the ability to analyze and screen therapeutics targeting the tumor vasculature, including those other than hornerin, in a more time-effective manner.

Despite these improvements, however, there are certain limitations to our work. First, it must be noted that three different computers were used for analysis, so variations in model or age of computers could impact the time measurements. Additionally, the batch processing feature, as of now, only permits users to set one threshold for all images that will be analyzed. The threshold is used to filter the useful features from the images away from the noise. In our analysis, all images were analyzed at a constant threshold of 30. However, this set threshold means that each individual image was not processed at its optimal threshold when conducting batch processing. As such, though the processing times are significantly quicker compared to manual processing, image analysis accuracy may be affected due to the constant threshold limitation. To address this, an algorithm to assign appropriate thresholds for each image during batch-processing can be implemented in the future.

The optimized RAVE software, though still subject to further updates, allowed us to characterize the effect of hornerin knockdown on the tumor vasculature in B16 melanoma. In order to characterize the effect of hornerin knockdown, we were first interested to see which regions after treatment with hornerin siRNA saw a significant

decrease in hornerin expression. Since siRNAs are negatively charged large molecules, it is difficult for the molecules to cross the cell membranes. Further, they undergo rapid degradation by plasma enzymes and are easily subjected to quick renal clearance sequestration.[14] To this end, our first sub-aim of the second aim looked into the levels of hornerin expression in different treatment locations, specifically by measuring mean gray intensity and integrated density on ImageJ. As seen in Figure 4, hornerin expression was reduced in endothelial cells in four of the five hornerin siRNA groups, namely M3-4, M3-5, M5-2, and M6-4, compared to the scramble siRNA group. The reduction in hornerin expression was significant in the M5-2 and M6-4 hornerin siRNA groups. Due to these results, we found that hornerin expression, as a result of hornerin siRNA treatment, was significantly decreased in two of the five hornerin siRNA groups. This confirmed the efficacy of hornerin siRNA in significantly downregulating the expression of the protein, specifically in two treatment locations. One limitation of this sub-aim, however, was the size and quantity of image samples that were analyzed. Due to delays in image acquisition, only 33 hornerin siRNA samples and 17 scramble siRNA samples from confocal imaging were analyzed. The sample sizes of the two groups were equal and were relatively small, possibly skewing our average values due to outliers. As such, in the future, more images could be analyzed for more comprehensive results.

We focused on the two hornerin siRNA (M5-2 and M6-4) groups as we moved forward to our second sub-aim. We were interested in characterizing the extent of vessel normalization in regions where hornerin expression was significantly decreased. Using the optimized RAVE software and our findings from the first-sub aim, we obtained the four vessel parameters across the five experimental groups, as seen in Figures 5 and 6. We found a reduction in vessel volume fraction, vessel length density, and fractal dimension between the two hornerin siRNA and scramble siRNA groups. For radius distribution, we found a higher frequency of M5-2 hornerin siRNA and M6-4 hornerin siRNA vessels in the 2-4 radius range, confirming that hornerin knockdown reduced the vessel radius size compared to the scramble siRNA group. Additionally, we saw a decrease in the three parameters of VVF, VLD, and FD between the vehicle and AV951 groups. As mentioned previously, all five groups were not compared together as the administration routes differed between the vehicle and AV951 treatments and the siRNA treatments. Furthermore, the lack of statistical significance between the vehicle and AV951 groups across the three parameters can be attributed to the dosage of AV951, which may not be the optimal dosage in melanoma. This reflects back to our rationale of identifying targets other than VEGF, such as hornerin. Overall, from these findings, we concluded that hornerin is an effective target for tumor vessel normalization through knockdown in regions where hornerin expression is significantly decreased. As such, in regions where hornerin expression is significantly reduced and vessel parameters are normalized, future work includes characterizing the downstream immune response. As mentioned in the introduction, the disordered tumor vasculature restricts T-cell entry into the tumor region. Therefore, following hornerin knockdown and subsequent vessel normalization, further studies can assess if T-cell infiltration is increased into the tumor region and a reduction in tumor volume is observed. This would offer a comprehensive review of the effect of hornerin knockdown not only on the vasculature, but on the tumor microenvironment as a whole. Ultimately, these findings would illuminate hornerin as a feasible target in development of a novel immunotherapeutic cancer drug, not limited to melanoma, but against a broad spectrum of cancers.

Materials and Methods

Rapid Analysis of Vessel Elements (RAVE)

Rapid Analysis of Vessel Elements, or RAVE, is a MATLAB graphical user interface (GUI) that allows for analysis of various vessel parameters.[11] For the scope of our project, parameters of vessel volume fraction, vessel length density, fractal dimension, and radius distribution were extracted. The optimized RAVE interfaced included correction of initial image loading error, exportable file, and batch processing.

When images were first inputted into RAVE and the “Browse” button was called, there was no processing of the images that occurred. The interface would prevent the display of results until the user switched the “Select Color” option between red and green multiple times. To address the loading error, we ran through the code, debugging to see what led to the error. We found that the “Browse” button callback, responsible for initializing the Graphical User Interface (GUI) once the image is added, was missing a function call, meaning that uninitialized variables were being referenced. A separate file titled VesselVolFrac.m was used to complete most of the processing. By calling on this VesselVolFrac function within the “Browse” button callback function, the required parameters were all properly initialized and the bug was fixed.

To address the lack of ability to output parameter data, we implemented a function that could output vessel

volume fraction, vessel length density, fractal dimension and the radius distribution data for each image. To begin, a button titled "Clear File" is clicked to remove any existing data in the output.csv file. Next, images are loaded and once the processed parameter values show up within the GUI, the user can click the "Output Results" button to store all the previously mentioned parameters as a row in a file titled "Output.csv". This button works by gathering all the parameters outputted by VesselVolFrac.m and writing them to a csv file sequentially.

To address the manual processing requirement, we implemented batch processing by taking advantage of the output results feature that was designed separately. With batch-processing, all images were analyzed at a constant threshold of 30. The threshold was determined by individually analyzing a few representative images and seeing what threshold setting would minimize noise while also maximizing the signal captured from the images. Similar to the "Browse" button, another button was created titled "Batch Process" which when clicked opened a window similar to the "Browse" button that allowed users to select files, with the exception that multiple files could now be chosen. Once the files were selected, all the file names were stored in a cell array. A loop was then used to iterate through all the files, by loading each one, running the existing RAVE analysis algorithm, and storing the produced parameters as a row in a .csv file. This method allowed for much quicker processing by automating the entire process and making high throughput analysis more efficient.

ImageJ Pre-Processing of Images Prior to RAVE Input

The stained images, collected in .czi format, were pre-processed in ImageJ and exported as .jpeg files prior to analysis in RAVE, both in the pre-optimized and post-optimized versions. Pre-processing allowed for the image to be split in three channels: CD31 (in green), hornerin (in red), and DAPI (in blue). The CD31 images were saved individually and then exported into RAVE for further vessel analysis.

Hornerin Quantification via ImageJ

Stained images collected from confocal imaging were uploaded onto ImageJ in .czi format. First, the hornerin and DAPI channels were merged, and the resulting image was analyzed using a Z projection with the sum slices option to create a real image that is the sum of all of the slices in the image stack. Then, the channels were split and the hornerin stained channel was converted to an 8-bit image. Following this, the background was subtracted using a rolling ball radius of 50 pixels, and the mean grey intensity and integrated density were measured as indicators of level of hornerin expression.

Animals

All experiments were performed on female 6-8-week-old C57BL/6j mice purchased from The Jackson Laboratory (Bar harbor, ME). All animal experiments were approved by the Animal Care and Use Committee at the University of Virginia and conformed to the NIH "Guide for the Care and Use of Laboratory Animals in Research."

Cell Lines

B16-OVA obtained from Dr. Victor Engelhard (UVA) were grown in RPMI medium 1640 (Life Technologies, Carlsbad, CA) supplemented with 5% fetal bovine serum, 1% L-Glutamine, 15mM HEPES, and 10ug/mL Blastacidin. Cells were maintained in a humidified atmosphere containing 5% CO2 at 37℃.

Tumor Studies

For tumor implantation, B16-OVA cells were grown under standard culture conditions for 48 h prior to being trypsinized and enumerated. B16-OVA were suspended in 400,000 cells/100 µL Dulbecco's Buffered Saline (DPBS, Hyclone, Logan, UT). The mice were shaved on flank prior to tumor inoculation. The cell mixture containing 0.4 million B16-OVA was injected subcutaneously into C57BL/6j mice unilaterally on the flank. The injection site for subcutaneous tumors was monitored for tumor volume daily based on caliper measurements using the formula $(\text{width}^2 \times \text{length})/2$. Treatments were given when the tumor size reached 110 mm^3.[2]

The AV951 (VEGF inhibitor) treatment was given as previously described.[2] In brief, AV-951 (Selleck Chemicals, Houston, TX) was suspended in 0.5% methocel + 0.5% Tween-20 in HBSS. 50 µL of 1.5 mg/kg AV-951 or vehicle control solution was administered once daily through oral gavage (22-gauge gave needle (Kent Scientistic, Torrington, CT) connected to a 1 mL syringe) for 7 days.

For hornerin siRNA treatment, Hrnr Mouse siRNA Oligo Duplex (Origene; catalog number SR42759) and Trilencer-27 Universal scrambled negative control siRNA duplex (Origene; catalog number SR30002) were used for injection. 10 µg of hornerin or control siRNA were combined with in vivo-jetPEI transfection reagent (Polyplys, France) in solution with 5% glucose following manufacturer's instructions. After 30-minute incubation at room temperature, a total volume of 50 µL siRNA mixture was injected into the center of the tumor (30-gauge insulin

needle (BD, Franklin Lakes, NJ)), every other day for 7 days. An overview of the tumor study timeline is also shown in Figure 7.

Following completion of the treatment, the mice were euthanized, and the tumors were harvested and fixed in % PFA overnight at 4C, followed by incubation in 30% sucrose overnight, then embedded in Neg-50 Frozen Section Medium (Thermo Scientific, Waltham, MA). The tissue block was frozen over liquid nitrogen vapor and cut into 15 µm sections.

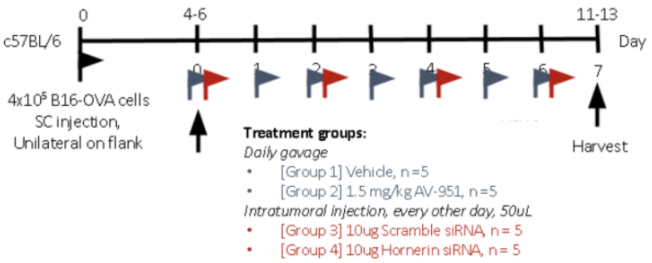

Figure 7: Tumor Study Timeline: Tumor cells were injected into mice on Day 1. Corresponding treatments were added starting when the tumor reached 110 mm^3 (Day 4-6 post tumor inoculation) and cross-sections were obtained on Day 7 post treatment.

Immunofluorescence Staining

Tumor sections were stained with CD31, DAPI, and hornerin. First, harvested tumors, across the varying experimental groups, were placed in the appropriate medium and treated with liquid nitrogen vapor until fully frozen. The tumors were then cryostat sectioned at 15 µm and stored at -80℃ until needed. The sectioned tumors then underwent immunofluorescence staining for CD31 and hornerin. The sectioned tumors were fixed, blocked, incubated with a primary and secondary antibody, which was fluorochrome-conjugated with AF594 and AF488 for hornerin and CD31, respectively. Lastly, the sections were stained for DAPI using Prolong Gold Antifade Reagent.

Confocal Imaging

Tumor sections stained with CD31, hornerin, and DAPI, were imaged using a Ziess LSM880 microscope and the ZEN image acquisition system. Images of the slides were all taken at 20x with a frame size of 1024x1024. The speed of image acquisition was 7, the gain was set at 750 for all three channels, with an airy unit of 1. The laser intensity for DAPI remained consistent around 10, while the CD31 and hornerin channel laser intensities were set at 30 for consistency across image acquisition. For each slide, two sections were imaged with two images in each section. After image acquisition, the file was saved in a .czi format.

Statistical Analysis

All statistical analyses performed were unpaired, two-tailed t-tests in order to compare the mean of two independent groups.

End Matter

Author Contributions and Notes

J.H conducted animal studies and performed immunofluorescence staining. J.H. and Z.A. conducted confocal imaging. S.R optimized the RAVE software. A.H performed hornerin quantification analysis. A.H, S.R and Z.A performed vessel analysis using RAVE, conducted statistical tests, and wrote the paper. The authors declare no conflict of interest.

Acknowledgements

We would like to thank our mentor, Jessica Hung, for all her help throughout our Capstone project. We would also like to thank our advisor, Professor Kimberly Kelly, for her feedback on our work throughout the year. Lastly, we would like to thank Elizabeth Wood, an undergraduate student in the Kelly Lab, who assisted with RAVE analysis.

References

1. Hanahan, D. & Weinberg, R. A. The hallmarks of cancer. *Cell* **100**, 57–70 (2000).
2. Gutknecht, M. F. *et al.* Identification of the S100 fused-type protein hornerin as a regulator of tumor vascularity. *Nat. Commun.* **8**, 552 (2017).
3. Cancer Statistics - National Cancer Institute. https://www.cancer.gov/about-cancer/understanding/statistics (2015).
4. Domingues, B., Lopes, J. M., Soares, P. & Pópulo, H. Melanoma treatment in review. *ImmunoTargets Ther.* **7**, 35–49 (2018).
5. Melanoma Skin Cancer Statistics. https://www.cancer.org/cancer/melanoma-skin-cancer/about/key-statistics.html.
6. Viallard, C. & Larrivée, B. Tumor angiogenesis and vascular normalization: alternative therapeutic targets. *Angiogenesis* **20**, 409–426 (2017).
7. Johnson, K. E. & Wilgus, T. A. Vascular Endothelial Growth Factor and Angiogenesis in the Regulation of Cutaneous Wound Repair. *Adv. Wound Care* **3**, 647–661 (2014).
8. Corrie, P. G., Basu, B. & Zaki, K. A. Targeting angiogenesis in melanoma: prospects for the future. *Ther. Adv. Med. Oncol.* **2**, 367–380 (2010).
9. Dana, H. *et al.* Molecular Mechanisms and Biological

Functions of siRNA. *Int. J. Biomed. Sci. IJBS* **13**, 48–57 (2017).
10. Takaishi, M., Makino, T., Morohashi, M. & Huh, N. Identification of Human Hornerin and Its Expression in Regenerating and Psoriatic Skin. *J. Biol. Chem.* **280**, 4696–4703 (2005).
11. Seaman, M. E., Peirce, S. M. & Kelly, K. Rapid Analysis of Vessel Elements (RAVE): A Tool for Studying Physiologic, Pathologic and Tumor Angiogenesis. *PLOS ONE* **6**, e20807 (2011).
12. Mauna Kea Technologies. https://www.maunakeatech.com/en/news-events/166-mauna-kea-technologies-receives-fda-510-k-clearance-of-cellvizio-with-a-fluorescent-dye-fluorescein-as-drug-device-combination.
13. An immunologist's guide to CD31 function in T-cells | Journal of Cell Science. https://jcs.biologists.org/content/126/11/2343.
14. Lamberti, G. & Barba, A. A. Drug Delivery of siRNA Therapeutics. *Pharmaceutics* **12**, (2020).

Supplemental Material:

0.098748	0.014232	1.392981	0.065141	0.37362	0.182234	0.113055	0.111171	0.044684	0.028802	0.021265	0.01319	0.01319	0.010229	0.013997	0.003096	0.00175	0.004576	0
0.030956	0.003708	0.983417	0.054847	0.317177	0.167942	0.135629	0.132653	0.055272	0.02381	0.027636	0.019983	0.004677	0.003827	0.01148	0.008503	0.015731	0.020833	0
0.010518	0.001735	0.842249	0.077899	0.402174	0.203804	0.146739	0.081522	0.020833	0.020833	0.021739	0.007246	0.006341	0	0.009058	0	0	0.001812	0
0.049756	0.006522	1.221617	0.039628	0.341243	0.222358	0.150196	0.10592	0.040117	0.023973	0.032779	0.015166	0.005871	0.005871	0.004892	0.008806	0	0.00318	0
0.03118	0.004939	1.69983	0.056979	0.437443	0.236961	0.124812	0.07356	0.014471	0.012662	0.014471	0.008743	0.004522	0.001809	0.003015	0.002713	0.004522	0.003316	0
0.030889	0.005597	1.095289	0.077381	0.440826	0.220938	0.095588	0.07458	0.019258	0.02556	0.019258	0.009104	0.007003	0.003501	0.003852	0.002101	0.00035	0.0007	0
0.039476	0.008518	1.04631	0.125226	0.456653	0.192354	0.077664	0.070439	0.010536	0.015352	0.021674	0.010536	0.005418	0.003612	0.003311	0.003612	0.002107	0.001505	0
0.054237	0.01047	1.206125	0.098307	0.406078	0.184173	0.106058	0.096064	0.028554	0.014685	0.024883	0.00877	0.006731	0.004079	0.007138	0.009994	0.000612	0.003875	0
0.458593	0.058326	1.770177	0.103344	0.316963	0.153873	0.099878	0.101493	0.054665	0.028987	0.044071	0.027254	0.014533	0.010279	0.016502	0.011106	0.006538	0.010516	0
0.038396	0.005025	1.055516	0.088094	0.311425	0.200275	0.091191	0.142808	0.044391	0.036132	0.032003	0.014109	0.009979	0.008259	0.007571	0.005506	0.003441	0.004818	0
0.053176	0.007597	1.182231	0.087829	0.354839	0.154784	0.096503	0.087558	0.044185	0.031174	0.037409	0.027921	0.02765	0.004608	0.014638	0.005422	0.01247	0.013012	0
0.065951	0.009823	1.150768	0.080142	0.354677	0.160494	0.092906	0.095208	0.053986	0.033898	0.040176	0.020088	0.017368	0.012136	0.018832	0.012764	0.002092	0.005231	0
0.044744	0.007593	1.137038	0.090375	0.332653	0.216492	0.129436	0.100332	0.045954	0.020168	0.019147	0.010978	0.003574	0.004595	0.00817	0.009191	0.001532	0.007404	0
0.02768	0.004384	1.703842	0.064842	0.366316	0.253053	0.151579	0.069895	0.026105	0.023158	0.018105	0.005053	0.009684	0.002526	0.005895	0.001263	0.002105	0.000421	0
0.047219	0.006252	1.771136	0.081736	0.344304	0.177939	0.092948	0.104521	0.052441	0.025316	0.039783	0.013743	0.024955	0.012658	0.008318	0.008318	0.002893	0.010127	0

Figure S1: RAVE Output .csv File: The image demonstrates a representative output. csv file from RAVE after batch processing. The columns, in order, provide values for vessel volume fraction, vessel length density, fractal dimension, and frequencies of radii from 0-2 pixels increasing to 30+ with each radii being placed into a 2-pixel wide bin.

Email Signature Screenshots